Broken C-shaped extinction curve and near-limit flame behaviors of low Lewis number counterflow flames under microgravity

Broken C-shaped extinction curve and near-limit flame behaviors of low Lewis number counterflow flames under microgravity

Authors: Tomoya Okuno[1], Takaki Akiba[1], Hisashi Nakamura[1], Roman Fursenko[2], Sergey Minaev[2], Takuya Tezuka[1], Susumu Hasegawa[1], Masao Kikuchi[3], and Kaoru Maruta[1,2]

Affiliations: 1. Institute of Fluid Science, Tohoku University,

2-1-1 Katahira, Aoba-ku, Sendai, Miyagi 980-8577, Japan.

2. Far Eastern Federal University,

8 Suhanova St., Vladivostok, 690950, Russia

3. Japanese Aerospace Exploration Agency,

2-1-1 Sengen, Tsukuba, Ibaraki 305-8505, Japan.

Type of article: full-length

Corresponding author: Tomoya Okuno

TEL: +81-22-217-5296

FAX: +81-22-217-5296

E-mail: okuno@edyn.ifs.tohoku.ac.jp

Abstract

To examine the effect of Lewis number on the extinction boundary, flame regimes, and the formation of sporadic flames, microgravity experiments on counterflow flames for $CH_4/O_2/Kr$ ($Le \approx 0.7\text{-}0.8$) and $CH_4/O_2/Xe$ ($Le \approx 0.5$) mixtures, and three types of computations, which are one-dimensional computations with a PREMIX-based code using detailed chemistry, and three- and one-dimensional computations with the thermal-diffusion model using an overall one-step reaction were conducted. In the microgravity experiments, planar flames, planar flames with propagating edges, planar flames with receding edges, star-shaped flames, cellular flames, and sporadic flames were identified, and their regions of existence in the equivalence ratio-stretch rate plane were obtained. Sporadic flames were formed for Xe mixtures but not for Kr mixtures in the experiments. Similarly, sporadic flames were formed at $Le = 0.50$ but not at $Le = 0.75$ in the three-dimensional computations with the thermal-diffusion model. Also, the flame regime of sporadic flames extended far beyond the extinction boundaries obtained in the one-dimensional computations in both experiments and the three-dimensional computations. Furthermore, a comparison of the sporadic flames and flame balls in the three-dimensional computations showed that sporadic flames are intermediate combustion modes that segue flame balls to propagating flames.

1. Introduction

Studies on the dynamics and the combustion limits of premixed flames are essential fundamentals for the development of clean combustion technologies such as lean-burn engines. However, a complete and comprehensive understanding on the dynamics and the combustion limits of near-limit stretched premixed flames has not yet been achieved for low Lewis numbers, despite extensive efforts of many researchers. The combustion limits of stretched premixed flames have been widely studied using flames in stagnation flow or counterflow fields [1–10]. Experimental investigations on the combustion limits at low stretch rates have been conducted under microgravity [7,9,10], in order to minimize disturbance to the flame caused by natural convection. These studies have been conducted over a range of Lewis numbers, Le, from 0.97 to 1.8, but studies for even lower Lewis numbers are still scarce.

Focusing on this issue, we have previously conducted counterflow experiments under microgravity using $CH_4/O_2/Xe$ mixtures ($Le \approx 0.5$) at stretch rates from 1.1 to 4.4 s^{-1} [11–13]. We have also conducted experimental investigations under microgravity with the effect of radiation reabsorption at slightly higher Lewis numbers ($Le \approx 0.75$) using $CH_4/O_2/CO_2$ mixtures [14]. In these previous studies, we have shown that transitions to ball-like flames from counterflow planar flames occur at extremely low stretch rates [11–14]. Extension of the combustion limit due to the formation of multiple ball-like flames, termed sporadic flames, has also been obtained in the framework of the thermal diffusion model [13]. Sporadic flames are a group of ball-like flames,

3

which are formed when each cap-like segment in a cellular flame breaks up and close upon themselves [15–18]. Similar flames have also been reported to exist in uniform flows[15–21], tubes [22–25], divergent channels [26], and Hele-Shaw cells [27]. However, the difficulty in experimental observation of these flames which are free from the effect of conductive heat loss or disturbance from natural convection has resulted in incomplete studies on these sporadic flames. Namely, the effects of Lewis number on the combustion limits, formation of sporadic flames, and flame regimes under microgravity remain largely uninvestigated. Therefore in this study, we aim to investigate this issue by using Kr or Xe gas as a diluent for methane and oxygen mixture to change the Lewis number.

Another type of flame that can be observed under microgravity is the flame ball. Flame balls are spherical flames without flame propagation which exist in quiescent mixtures at Lewis numbers sufficiently lower than unity. The existence of flame balls were first suggested by Zel'dovich [28] and was later verified by theoretical [29–31], computational [32–35], and experimental [36,37] investigations. A single ball-like flame in the sporadic flame resemble these flame balls in shape and in the conditions that these flames are formed. However, direct comparisons between the sporadic flames and the flame balls have not been conducted yet. Therefore in this study, we have additionally compared the flame structures, characteristic flame sizes, and the combustion limits of flame balls and the sporadic flames obtained with

computations in an attempt to clarify the relation between these two flames.

2. Experimental methods

Microgravity experiments were conducted to obtain the combustion limit, near-limit extinction boundary, and flame regimes of counterflow flames for mixtures with different Lewis numbers. Figure 1 shows a schematic of the experimental apparatus.

The microgravity environment was attained by parabolic flights of an airplane (MU-300) operated by Diamond Air Service Incorporation [38], Japan. The duration of microgravity was around 15–20 seconds, and the gravity levels were on the order of ±0.01 G. In the present study, data were removed for consideration when the gravity level exceeded 0.1 G during the microgravity experiments. To conduct the counterflow flame experiments, two opposed cylindrical burners were placed inside a chamber. Here, the burner inner diameter was 30 mm and the burner distance was from 30 to 45 mm. The burner distance was changed depending on the stretch rate to avoid upstream conductive heat loss to the burners from the flames. A detailed description of the experimental apparatus and the experimental procedure can be found in [7].

In the experiments, $CH_4/O_2/Kr$ or $CH_4/O_2/Xe$ premixtures were supplied to both burners, forming a counterflow field. The mole fraction ratio of O_2 to the diluents in the mixtures were set to 0.14. Lewis numbers for Xe and Kr mixtures were around 0.5 and 0.7‑0.8, respectively.

Separate mass flow controllers were used to control the flow rates for each gas component of the mixtures. Each mass flow controller was calibrated before and after each flight using a flow meter (Horiba SF-1U) to ensure that no changes in the applied voltage-flow rate conversion factor occurs due to the acceleration during the flight. The accuracy of the flow meter measurement is within ± 1.0 % of the reading point. This results in around ± 2.0 % uncertainty in the equivalence ratio and ± 1.0 % uncertainty in the stretch rate.

After ignition, the equivalence ratio ϕ and/or the stretch rate a were gradually changed to obtain extinction. Here, the global stretch rate was defined as $a = 2U/L$ where U is the mean velocity at the burner outlet and L is the burner distance. In most cases, the stretch rate was kept constant and the equivalence ratio, ϕ, was gradually decreased by 0.015 per second. For flame observation, two HD cameras and a high-speed camera equipped with an image intensifier (Photron FASTCAM MC2.1) were used. Equivalence ratio at extinction was defined as the instantaneous equivalence ratio when the chemiluminescence from flames vanished in the camera image by considering flow residence time from mass flow controllers to the counterflow field. To check the effect of the G-jitter, counterflow flame extinction experiments using CH_4/air mixtures were conducted, and a good agreement between the extinction boundaries obtained with the droptower and the airplane experiments were found. Supplementary video files of the droptower and airplane experiments are also provided to demonstrate the small effect of the G-jitter.
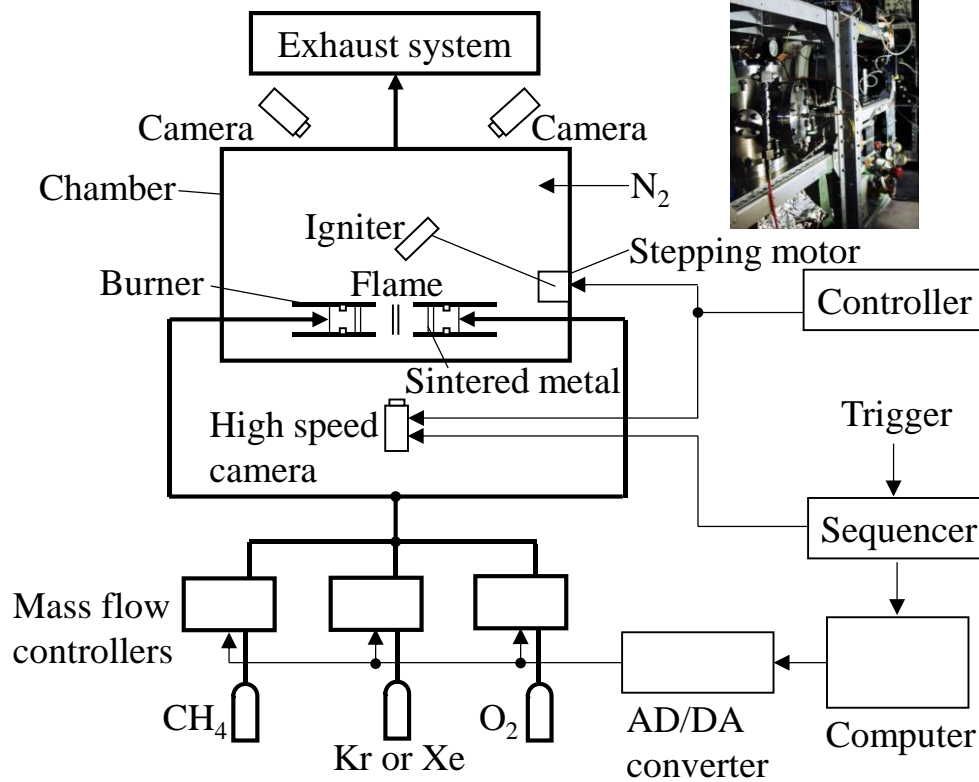
Fig. 1 Schematic and a picture of the experimental setup [7].

3. Computational methods

We have conducted three types of computations in this study: one-dimensional computations with a PREMIX-based code using detailed chemistry, and three- and one-dimensional computations with the thermal-diffusion model using an overall one-step reaction.

One-dimensional computations with a PREMIX-based code using detailed chemistry for ideal steady-state planar counterflow flames [10] were conducted to obtain the C-shaped extinction boundary and their results were compared with the experimental results. The optically

thin model was used for the radiation heat loss from the flames to the ambient [10]. All computations were conducted under atmospheric pressure. GRI-Mech 3.0 [39] without nitrogen reactions was used for the chemical mechanism. Thermodynamic [40] and transport [41] properties for Xe and Kr were added, and the third-body collision coefficients of Ar were used for Xe and Kr. GRI-Mech 3.0 without nitrogen reactions including Xe was used for $CH_4/O_2/Xe$ mixtures in [42], and sufficiently accurate results were obtained even at equivalence ratios near the lean combustion limit. From this, similar accuracy is expected for $CH_4/O_2/Kr$ mixtures due to the similar molecular structure between Kr and Xe. Computations using the same chemical mechanism showed that the flame temperatures of Kr and Xe flames were 1462 and 1448 K, respectively, and the flame propagation velocities of Kr and Xe flames were 3.58 and 2.62 cm/s, respectively, at $\phi = 0.62$ for the radiative planar unstretched flame.

Three-dimensional computations with the thermal-diffusion model and an overall one-step reaction for counterflow flames used in [13] were employed to obtain the flame regimes and to qualitatively compare with the experimental flame regimes. Here, transient non-dimensional equations describing the fuel concentration and the temperature [13] were solved with the constant density assumption and a given flow field, and the governing equations are as follows.

$$\frac{\partial T}{\partial t} + \vec{V}\nabla T = \nabla^2 T - h(T^4 - \sigma^4) + (1 - \sigma)W(T, C) \qquad (1)$$

$$\frac{\partial C}{\partial t} + \vec{V}\nabla C = Le^{-1}\nabla^2 C - W(T, C) \qquad (2)$$

The units for temperature, T, and the fuel concentration, C, are the adiabatic flame temperature, T_b, and the initial gas concentration, C_0, respectively. The unit for the distance is the flame thickness l_{th} obtained from $l_{th} = D_{th}/U_b$, where D_{th} is the thermal diffusion coefficient and U_b is the laminar burning velocity of the adiabatic planar unstretched flame. The unit for time, t, is D_{th}/U_b^2.

The ambient temperature, σ, was defined by $\sigma = T_0/T_b$, where T_0 was 300 K. The Lewis number, Le, is defined as D_{th}/D_{mol} where D_{mol} is the fuel molecular diffusivity. The velocity field $\vec{V}$ was given as $\vec{V} = (AX/2, -AY, AZ/2)$ assuming a potential flow field and A is the non-dimensional stretch rate. The radiation heat loss to the ambient is considered, and the unit for the scaled Stephan-Boltzmann constant, h, is $\rho_b c_p l_P U_b / 4 T_b^3 l_{th}$. Here, ρ_b is the burned gas density, c_p, is the specific heat, and l_P is the Plank mean absorption length. The same radiation heat loss parameters as [13] were used. For the chemistry, we have employed the single reactant one-step Arrhenius-type exothermic reaction for fuel-lean mixtures where $W(T, C) = (1 - \sigma)^2 N^2 C \exp(N(1 - 1/T))/2Le$. N is the nondimensional activation temperature which is defined as $N = T_a/T_b$. T_a is the activation temperature. Computations with the thermal-diffusion model was conducted due to the high computational cost in resolving the wide range of spatiotemporal scales of sporadic flames in the counterflow field. The computed domain in nondimensional values were set to be $-40 \leqq X \leqq 40$, $-30 \leqq Y \leqq 30$, and $-40 \leqq Z \leqq 40$. The mixtures flow into the computational domain from the planes $Y = \pm 30$, and flow out from the planes $X = \pm 40$ and $Z = \pm 40$. The boundary

conditions at the mixture inlet were $T = \sigma$, $C = 1$, and the boundary conditions at the mixture outlet were $T = \sigma$, $C = 0$. Fixed boundary conditions were used to express far field boundary conditions for the sporadic flame. The fuel concentration gradient near the mixture outlet boundary condition did not affect the results near the center of the computational domain due to the large domain size, and only the results away from these gradients are used for discussions throughout this paper.

To convert the non-dimensional values to dimensional values, the relation $U_b = B\exp(-T_a/2T_b)$ formulated for planar adiabatic flames in the high activation energy limit was used [28]. To obtain U_b, first, the activation temperature T_a was set to a certain value. Then, T_b as a function of equivalence ratio was fitted to the results obtained by PREMIX with GRI-Mech 3.0 at $0.38 \leqq \phi \leqq 0.6$ for $CH_4/O_2/Xe$ mixtures. Next, B was changed to fit the equivalence ratio dependence of U_b near the lean limit. If a good fit for U_b could not be obtained, T_a was modified. As a result, $T_a = 15000$ K and $B = 300$ were used. In the computations, an orthogonal uniform grid with grid numbers $384 \times 284 \times 384$ were applied, which results in the non-dimensional grid spacing of around 0.21. The dependence of grid spacing on the adiabatic flame propagation speed and the flame shape was found to be negligible below 0.21, e.g., 0.2 % difference in flame propagation speed with the grid spacing of 0.10. The non-dimensional time step was set to 1.0×10^{-4}. Initially, the computational domain was filled by unburnt gas mixture

at atmospheric temperature and a spherical hot zone was specified near the center to ignite the mixture. However, this method results in an early flame extinction near the limits. Therefore, in order to obtain the solutions for flames near the combustion limits, the results slightly away from the limit were used as an initial condition, and σ or non-dimensional stretch rate A was gradually changed to the desired condition.

Three-dimensional computations with the thermal-diffusion model in a quiescent mixture for ideal flame balls were also conducted to further investigate the relation between sporadic flames and flame balls. For these computations, the computational domain was set to -50$\leqq X \leqq$50, -50$\leqq Y \leqq$50, -50$\leqq Z \leqq$50 and the grid numbers were 479$\times$479$\times$479 with the non-dimensional grid spacing of around 0.21. At the boundaries, the temperature and fuel concentration was fixed as $T = \sigma$, and $C = 1.0$. The dependences of the domain size above 100 and grid spacing below 0.21 on the flame ball size and temperature were found to be negligible, e.g., differences of 0.9 % in flame ball temperature and 0.4 % in flame ball radius with smaller grid spacing of 0.17, and 0.1 % in flame ball temperature and 1.5 % in flame ball radius with larger domain size of 120. The computations for flame balls were continued until steady-state solutions were obtained. For the initial conditions, a point-symmetric temperature profile based on the temperature profile of the sporadic flame in the burner axial direction at $A = 0.007$ were used since the sporadic flame was nearly spherical at these low stretch rates.

One-dimensional computations with the thermal-diffusion model using an overall one-step reaction for the ideal planar counterflow flames were conducted to obtain the C-shaped extinction boundary and compare with the combustion limits obtained in the three-dimensional counterflow flame computations. The same parameters with the three-dimensional computations were used. Computations at higher stretch rates were conducted using smaller grid spacing due to the thin reaction zone in these conditions.

4. Experimental and computational flame patterns

Figure 2 shows the experimental flame images during two typical experimental sequences at stretch rates $a = 3.2$ s^{-1}. These images were taken from the high speed camera with an image intensifier from the orthogonal direction to the burner axis. The dashed lines indicate the cylindrical burner outlet ports. The mixtures were ignited at higher equivalence ratios and the equivalence ratio was gradually decreased until extinction by keeping the stretch rate constant. For the Kr mixture (Fig. 2(a)), the flames are planar for equivalence ratios $\phi = 0.52$–0.48. The image at $\phi = 0.46$ for the Kr mixture was taken right before extinction resulting in a non-planar
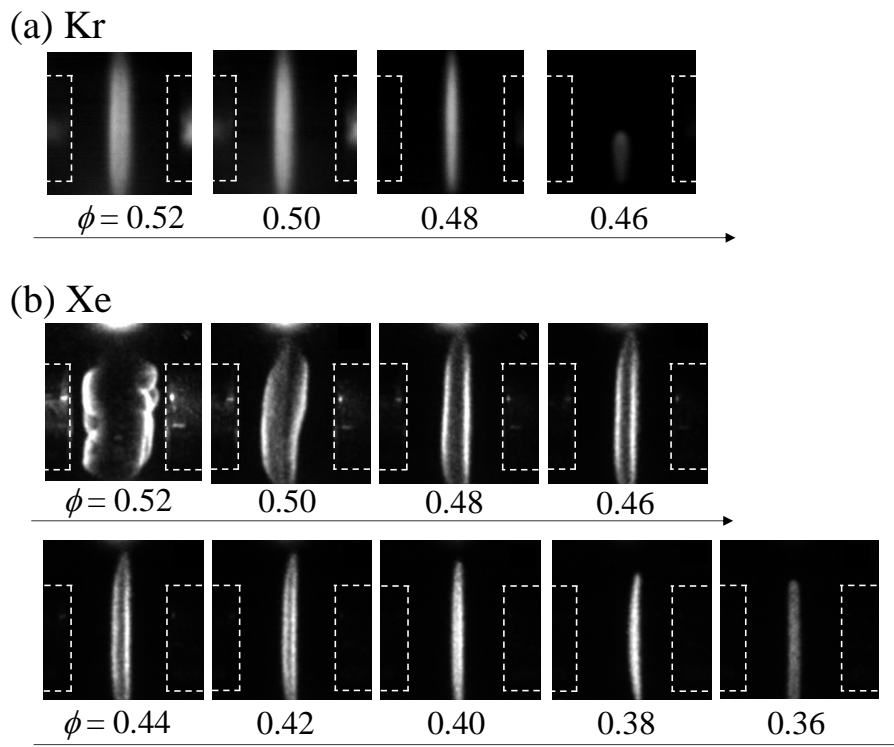

(a) Kr

$\phi = 0.52$ 0.50   0.48   0.46

(b) Xe

$\phi = 0.52$ 0.50   0.48   0.46

$\phi = 0.44$ 0.42   0.40   0.38   0.36

Fig. 2 Experimental flame images at stretch rate $a = 3.2$ s^{-1} for Kr mixtures (a), and Xe mixtures (b).

shape which will be discussed later. The flame is cellular and non-planar for the Xe mixture at ϕ

= 0.52 and 0.50 (Fig. 2(b)). As the equivalence ratio decreases, the cellular flame becomes planar.

The formation of the cellular flames for the Xe mixture is due to the occurrence of diffusive-

thermal instability, attributed to the lower Lewis number of Xe mixtures ($Le \approx 0.5$ for Xe mixtures,

and $Le \approx 0.7$–0.8 for Kr mixtures). The disappearance of the cells at lower equivalence ratios is

in accordance with the previous study [13]. For Xe mixtures, the flames extinguish around ϕ =

0.38, which is much smaller than the equivalence ratio at extinction for the Kr mixture at the same

stretch rate. This is due to the Lewis number effect. Similar to the experimental result for the Kr

mixture, a non-planar flame was also observed for the Xe mixture just before extinction, which

will also be discussed later.

The instantaneous flame images taken from different experimental sequences at $\phi = 0.48$

for a = 3.2 and 2.1 s^{-1} with Kr mixtures, and for a = 3.2, 2.2 and 0.82 s^{-1} with Xe mixtures are

shown in Fig. 3. For Kr mixtures, the flames are planar at stretch rates a = 3.2 and 2.1 s^{-1}. For the

case of a = 2.1 s^{-1}, the flame is close to extinction. However, for the case of Xe mixtures, the

flames are planar at a = 3.2 s^{-1}, but become cellular at a = 2.2 and 0.82 s^{-1}. Particularly at a = 0.82

s^{-1}, all the cells are separated which may lead to reactant leakage from the flame front to the

stagnation plane. These flames are called sporadic flames and have been reproduced by

computations with the thermal-diffusion model in [12,13]. Here, the size of each cell in the radial

direction is around 10 to 25 mm. Sporadic flames were not observed for Kr mixture flames for
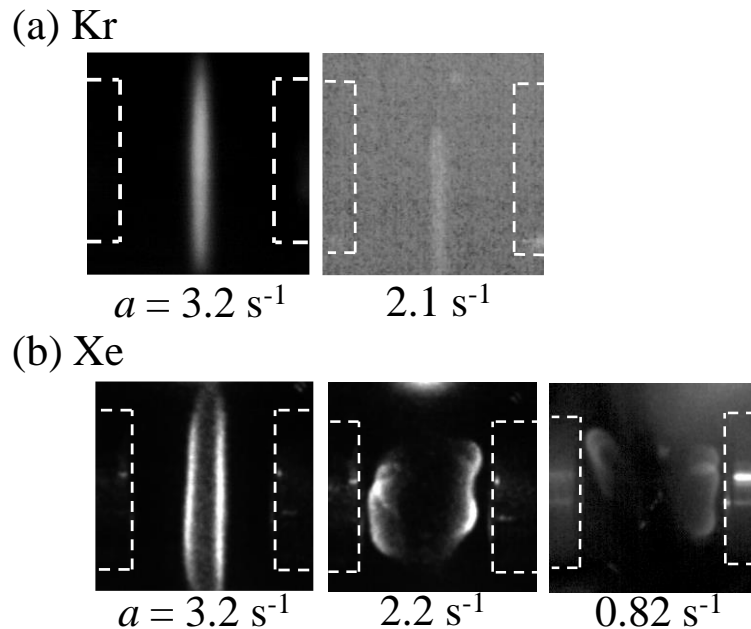

Fig. 3 Experimental flame images at equivalence ratios $\phi = 0.48$ and different stretch rates
for (a) CH$_4$/O$_2$/Kr mixtures and (b) CH$_4$/O$_2$/Xe mixtures.

any conditions investigated in the current study.

To demonstrate the behavior of sporadic flames, flame images of sporadic flames at $a =$ 0.82 s^{-1} and around $\phi = 0.39$ are shown in Fig. 4. Three ball-like flames are first formed at 5.8 s. With passing time, the flame on the left-hand side inside the image extinguishes, while one ball-like flame remains at 8.8 s. The ball-like flame pulsates and shifts which may be due to the asymmetric flame formation and the G-jitter. The ball-like flames survives for over 6 s until it is extinguished by the end of microgravity at around 12.3 s. The long lifetime of the sporadic flame experimentally indicates that sporadic flames are quasi-steady. However, longer microgravity duration is required to fully investigate the stability of such flames, characteristic lengths, and flame behaviors in the near future by space experiments scheduled for 2020 in the International Space Station.
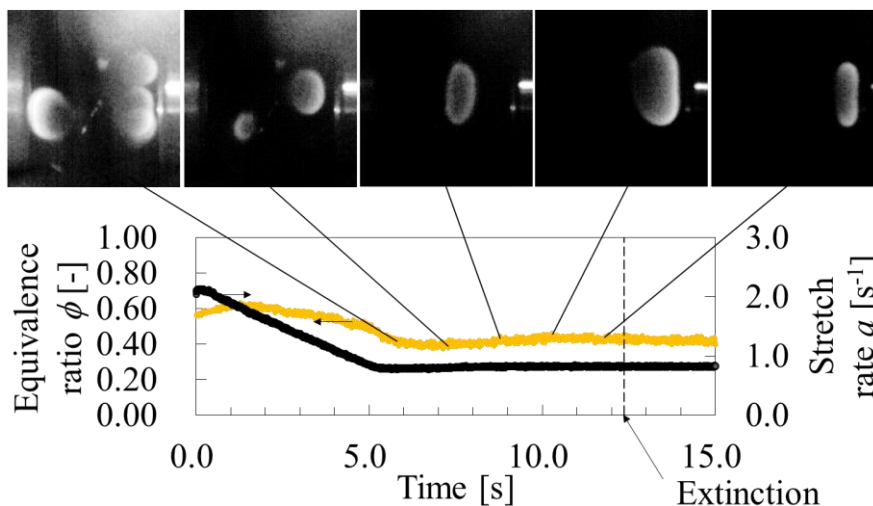

Fig. 4 Experimental flame images of sporadic flames at equivalence ratios $\phi = 0.39$ and stretch rate $a = 0.82$ s^{-1}.

Other than the three flame types already introduced, i.e., planar flames, cellular flames, and sporadic flames, additional three types of flames were experimentally observed both for Kr and Xe mixtures. Typical flame images of these additional three flames for Xe mixtures are shown in Figs. 5(a), 5(b), and 5(c). Near the extinction of planar flames, planar circular flames with receding edges (Fig. 5(a)), and planar circular flames with propagating edges (Fig. 5(b)) were observed, in addition to the instantaneous whole region extinction. In Figs. 5(a) and 5(b), time = 0 corresponds to the time that the flame edges starts to move. For the flame shown in Fig. 5(a), the merged edges of the planar circular flame recedes into the burnt gas. The flames then extinguish approximately after 1.2 s from the time that the flame edges started to move. This corresponds to the failure wave of the flame edges. For the flame shown in Fig.5(b), the merged edges move towards the unburnt gas and propagates at 0.0–0.5 s. When the merged edges move toward the unburnt gas, local extinction occurs and the flame is broken into the core section and the fragments moving further downstream at 0.5 s in Fig. 5(b). Possible causes for the local extinction are the effect of radiation heat loss and the radial conductive heat loss [43,44]. From 0.6-1.3 s in Fig. 5(b), the behavior changes as the equivalence ratio is slightly decreased where the flame pulsates in the radial direction and extinguishes soon after 1.3 s. It should be noted that the detailed investigation on the mechanisms for this behavior could not be conducted since the

17

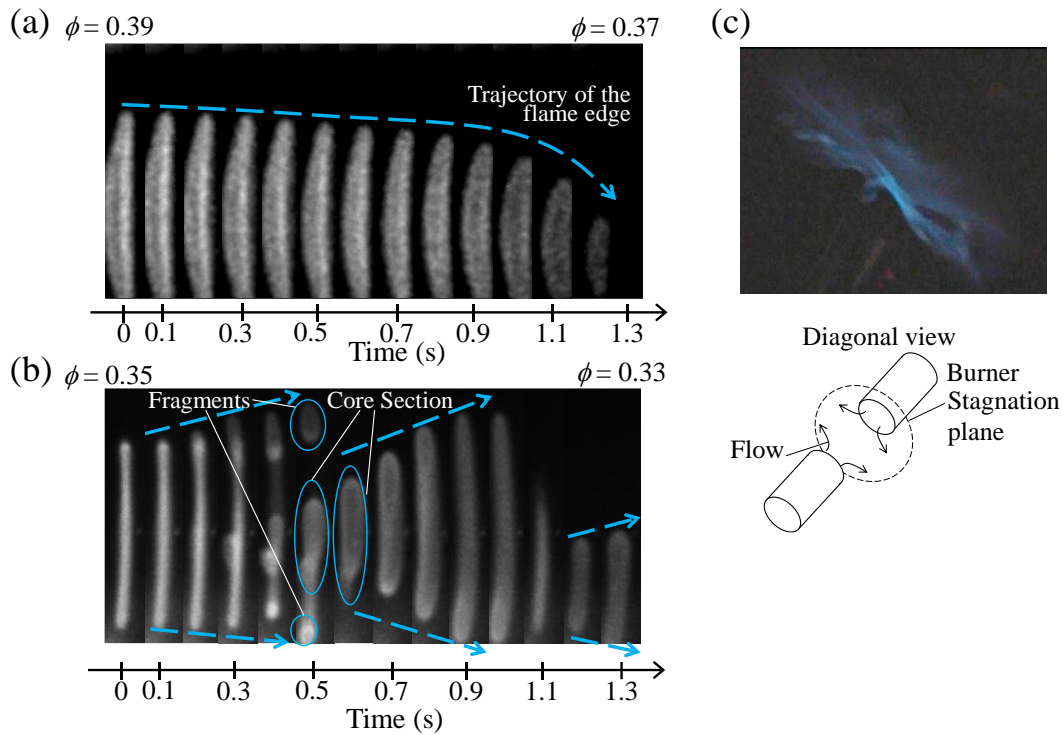effect of local stretch acting on the flame edges may not be completely uniform depending on the flame location.

Fig. 5 Time history of the experimental flame images for $CH_4/O_2/Xe$ mixtures. Planar circular flames with receding edges at $\phi = 0.37$ and $a = 2.7$ s^{-1} (a). Planar circular flames with propagating edges at $\phi = 0.35$ and $a = 3.2$ s^{-1} (b). Star-shaped flames (c).

At high stretch rates, star-shaped flames were observed as shown in Fig. 5(c) for Xe flames at $\phi = 0.74$ and $a = 14.9$ s^{-1}. The image is taken from the HD camera placed in a diagonal direction to the burner axis and the stagnation plane. The flame appears to have grooves along the stagnation plane, thus becoming star shaped. The flame also has wrinkles when seen from the direction along the stagnation plane although it is not shown here. The cause in the formation

mechanism of these flames are under consideration. Note that this is not due to flow turbulence

since a planar flame was obtained with the same setup for $CH_4/O_2/CO_2$ mixtures [14] and CH_4/air

mixtures at the same and higher stretch rate region up to 15 s⁻¹.

To compare with the experimental flame images, results obtained in the three-

dimensional computations with the thermal-diffusion model using an overall one-step reaction
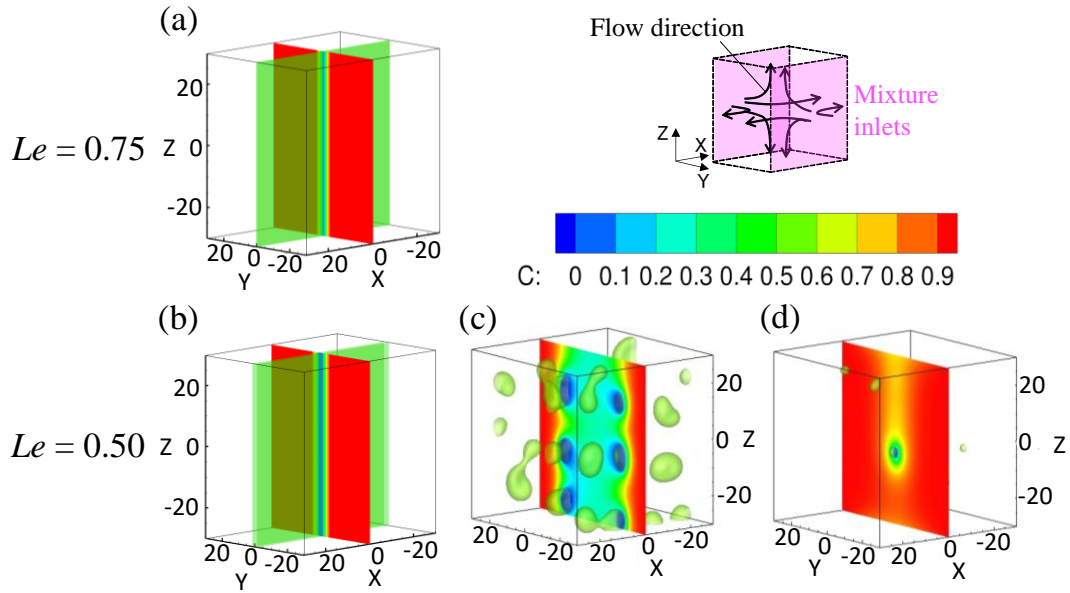

Fig. 6 Temperature iso-surfaces at $T = 0.75$ and fuel concentration contours at $X = 0$. (a) $Le = 0.75$, $\sigma = 0.234$, $A = 0.26$, $\phi = 0.48$, $a = 1.0$ s⁻¹, (b) $Le = 0.50$, $\sigma = 0.234$, $A = 0.26$, $\phi = 0.48$, $a = 1.0$ s⁻¹, (c) $Le = 0.50$, $\sigma = 0.234$, $A = 0.028$, $\phi = 0.48$, $a = 0.11$ s⁻¹, (d) $Le = 0.50$, $\sigma = 0.256$, $A = 0.028$, $\phi = 0.42$, $a = 0.035$ s⁻¹.

for counterflow flames are shown in Fig. 6. Here, temperature iso-surfaces at $T = 0.75$ and fuel

concentration contours at $X = 0$ are shown. $T = 0.75$ is the location where approximately 30–50 %

of the maximum heat release occurs in unstretched flames, which corresponds to the approximate

location of the reaction zone. At $\sigma = 0.234$ and $A = 0.26$ which is equivalent to $\phi = 0.48$ and $a =$

19

1.0 s^{-1}, planar flames are obtained for both $Le = 0.75$ and 0.50 conditions as shown in Figs. 6(a)

and 6(b). When the stretch rate is decreased, the flames extinguished from all zones at $Le = 0.75$

and $A = 0.23$ which is equivalent to 0.8 s^{-1}, although it is not shown here. Whereas for $Le = 0.50$,

the flames become sporadic flames at $\sigma = 0.234$ and $A = 0.028$ which is equivalent to $\phi = 0.48$

and $a = 0.11$ s^{-1}, as shown in Fig. 6(c). Here, the cells formed by the diffusive-thermal instability

is split into separate ball-like flames, and reactant leakage from the gap between the cells to the

stagnation plane is observed. Each cell splits or deforms, and is swept away due to the coupling

effect of the diffusive-thermal instability and the velocity field. However, these sporadic flames

are quasi-steady if the mean locations of flame propagation fronts are considered. This is

supported by the fact that extinction for all of the cells were not observed even after 500 unit times

equivalent to 131 s of computations in this condition, at $\sigma = 0.234$ and $A = 0.028$ equivalent to ϕ

$= 0.48$ and $a = 0.11$ s^{-1}. Figure 6(d) shows the temperature iso-surface and fuel concentration

contours at the same non-dimensional stretch rate ($A = 0.028$) with lower inlet fuel concentrations

of $\sigma = 0.256$ than the condition in Fig. 6(c). With the decrease in the inlet fuel concentration from

$\sigma = 0.234$ to $\sigma = 0.256$, the twin sporadic flames move closer together to form a single sporadic

flame. The merging of sporadic flames is similar to the behavior of flame balls which stand closer

than a critical distance [45]. At lower fuel concentrations of $\sigma = 0.256$, the gaps between each

ball-like flame also become wider than the ones in $\sigma = 0.234$. The decrease in the distance between

the sporadic flames interposing the stagnation plane, and the increase in the gaps between ball-like flames with the decrease in the inlet fuel concentration is also in correspondence with the previous results of three-dimensional computations [12]. In this condition, computations were also continued for 800 unit times equivalent to 627 s without flame extinction inside the whole domain. It should be noted that flame extinction over the entire computational domain was observed with a slight decrease in the inlet fuel concentration ($\sigma = 0.260$) at the same stretch rate ($A = 0.028$), or a slight increase in the stretch rate ($A = 0.036$) at the same inlet fuel concentration ($\sigma = 0.256$).

5. Comparison between flame balls and sporadic flames

To compare the characteristics of sporadic flames with that of flame balls, three-dimensional computations were conducted for examining the single ideal flame ball by neglecting the convection term in the governing equations of the thermal-diffusion model. Figure 7 shows the temperature contours (left) and fuel concentration contours (right) on the X-Y plane along $Z = 0$ (top) and the X-Z plane along $Y = 0$ (bottom) at $Le = 0.50$ and $\sigma = 0.256$ equivalent to $\phi = 0.42$. The result shown here is the solution at the steady state where the difference of the solution in time does not occur. The distance from the flame ball center to the point of maximum heat release rate is exactly the same in the X, Y, and Z-directions, and the center of the flame ball is located

very close to the origin of the coordinate. Thus, the current result can be regarded as an ideal

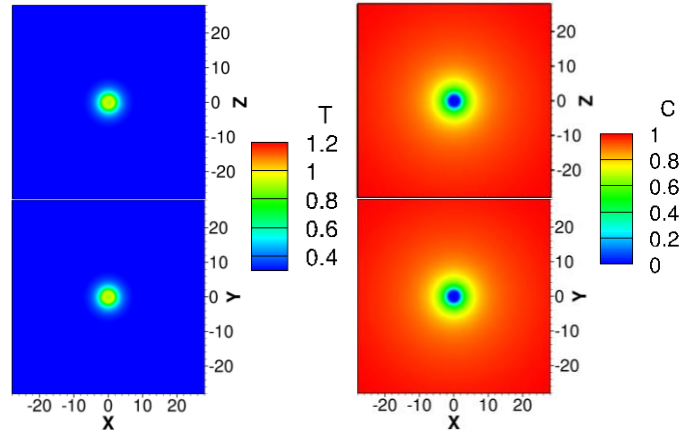spherical flame ball under the present parameters.

Fig. 7 Temperature contours (left) and fuel concentration contours (right) at $Y = 0$ (top) and $Z = 0$ (bottom) for $Le = 0.50$ and $\sigma = 0.256$ equivalent to $\phi = 0.42$.

Fig. 8 shows the comparison between the computed characteristic length distributions

of the sporadic flames and the flame ball diameter using temperature iso-surfaces at $T = 0.75$ as

representations of the flames. The characteristic lengths of the sporadic flames were obtained by

fitting ellipses by using the least square method [46] to the sporadic flames in the quasi-steady

state viewed along the burner axis. Both the major length and the minor length of the ellipsoid

were used. Only the sporadic flames in the region -28 $\leqq$ X $\leqq$ 28 and -28 $\leqq$ Z $\leqq$ 28 were

used to eliminate the effect of the outlet boundary on the flames. Over 10000 measurements are

typically present to make the size distribution for one condition. Also, the flames just before

splitting were separated using the watershed algorithm [47]. As can be seen in Fig. 8, the size

distribution of sporadic flames become narrower when non-dimensional stretch rate A becomes

lower at constant σ. This is because the deformation of the ball-like flame before splitting

becomes smaller and the rate of splitting for each ball-like flame becomes slower as A is decreased.

At the same time, the size distributions of sporadic flames become closer towards the flame ball

diameter with the decrease in A. In addition, the most frequently appearing sizes of the sporadic

flames are larger than the flame ball diameter, but become slightly closer towards the flame ball

diameter due to the shift in the size distribution with decreasing A. At $A = 0.028$ and different σ,

the size distribution for sporadic flames become wider at smaller σ (higher ϕ). This is due to the

larger effect of the diffusive-thermal instability at smaller σ. At the same time, the size distribution

and the most frequently appearing characteristic flame sizes of sporadic flames shift toward larger

characteristic flame sizes. The increase in characteristic flame size with the increase in the mixture

fuel concentration qualitatively agrees with the dependence of flame ball size to the mixture fuel

concentration [32]. Here, the most frequently appearing characteristic flame size is around 9

equivalent to 2.1 cm, which agrees to our experimental results at the same equivalence ratio

conditions. The behavior of characteristic flame size of the sporadic flames depending on the A

and σ, clearly indicate that sporadic flames are intermediate combustion modes that segue flame

balls to propagating flames. Note that a stable flame ball solution at $\sigma = 0.234$ was not obtained

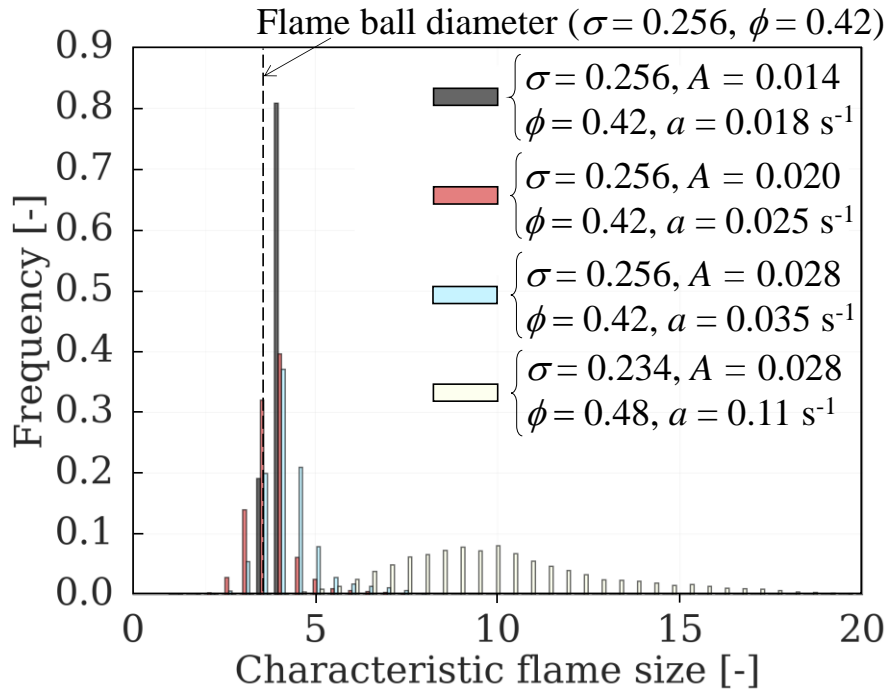due to the three-dimensional instability [29,48,49].

Fig. 8 Comparison between the distribution of the characteristic flame size for sporadic flames and the flame ball diameter.

Figure 9 shows the comparison between the flame structures at $\sigma = 0.256$ equivalent to $\phi = 0.42$ for the counterflow planar flame at $A = 0.26$ equivalent to 1.0 s^{-1}, sporadic flames at $A = 0.028$ equivalent to $a = 0.035$ s^{-1}, and the flame ball. Here, the results along $X = 0$ and $Z = 0$ are shown for the flame structures of the counterflow planar flame and the flame ball. The flame structures of sporadic flames are the result of eight measurements in the direction parallel to the burner axis near the center of the cells at different X, Z, and times. The figure shows that the
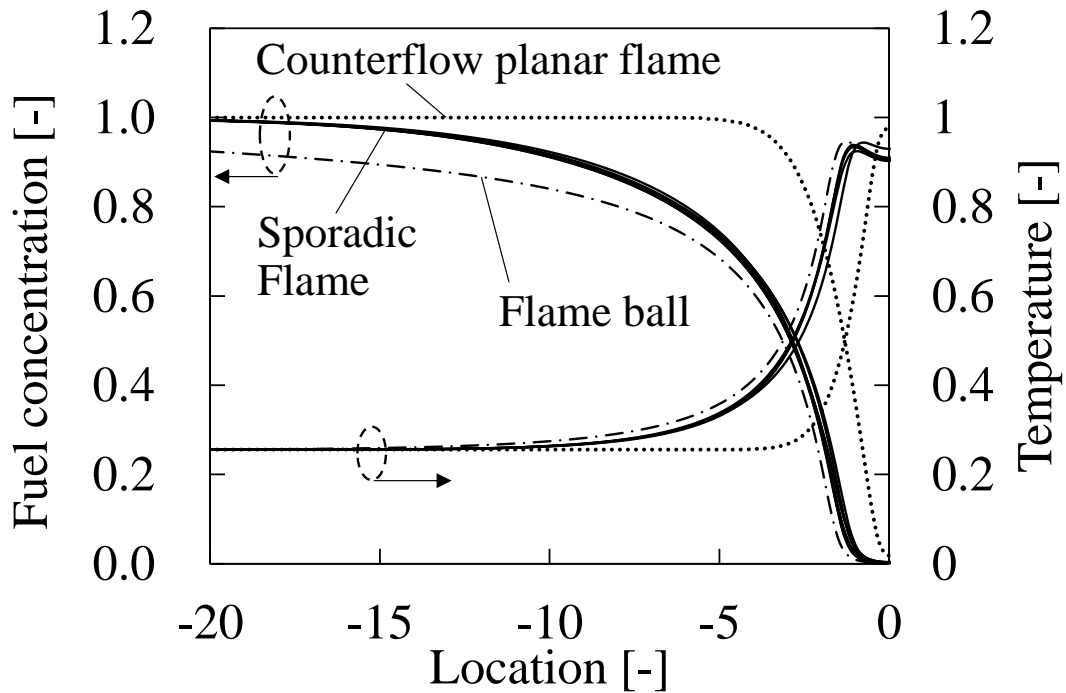
Fig. 9 Comparison of temperature and fuel concentration profiles for planar flames, sporadic flames, and flame balls at $\sigma = 0.256$ equivalent to $\phi = 0.42$. Dotted line indicates the results of planar flames at $A = 0.26$ equivalent to 1.0 s^{-1}, dashed and dotted lines indicate the result of the flame ball, solid lines indicate the results for sporadic flames at $A = 0.028$ equivalent to $a = 0.035$ s^{-1}.

sporadic flame structures have only small differences even at different locations and different times. In addition, the temperature profiles of sporadic flames are very close to the temperature profile of the flame ball, with the characteristic temperature profile of $T \propto 1/r$ in the preheat zone where r is the distance from the flame center. This shows that the sporadic flame is heavily under the influence of diffusion, similar to flame balls. The fuel concentration profile of sporadic flames close to the stagnation plane are very similar to that of the flame ball close to the center of the flame ball. However, the fuel concentration profile at the location away from the center of

sporadic flames do not agree with that far from the center of the flame ball. This is due to the

effect of the flow field. Figure 9 also shows that the distance between the location at the maximum

temperature of the sporadic flame and the stagnation plane is smaller than the flame ball radius.

Figures 8 and 9 show that the sporadic flames have slightly smaller characteristic flame sizes than

the flame ball in the axial direction, but have larger characteristic flame sizes in the direction

parallel to the stagnation plane.

6. Experimental and computational flame regime diagram

Figure 10 shows the experimental flame regimes, and the comparison between the

experimental extinction points and the C-shaped extinction boundaries obtained by the one-

dimensional computations using GRI-Mech 3.0 with the PREMIX-based code. The plots for the

experimental flame regime indicate the boundaries between different flame types, i.e., extinction

or transition into different flame types. Star-shaped flames are seen in both Kr and Xe mixtures

at conditions above a certain stretch rate regardless of the equivalence ratio condition, which

suggests that the star-shaped flames were not formed by the diffusive-thermal instability. In the

experiments, sporadic flames are seen in only Xe mixtures. Planar flames, planar flames with

propagating edges, planar flames with receding edges, and cellular flames are seen in both Kr and

Xe mixtures. The region of cellular flames for Xe mixtures are larger than the one for Kr mixtures.

This further indicates that the cellular flame is formed by the diffusive-thermal instability. Near the limit of the planar flames, planar flames with propagating edges were seen at $a > 3.0$ s^{-1}, whereas planar flames with receding edges were seen at $a < 3.0$ s^{-1}. This means that the propagation direction of the edge of the planar flame changes depending on the stretch rate. Except the stretch rate conditions where star-shaped flames were observed, the experimental extinction points of Kr mixtures showed very good agreements with the C-shaped extinction boundary obtained by the one-dimensional computations with the PREMIX-based code using detailed chemistry. In these conditions, the equivalence ratio at extinction for the same stretch rate deviated within 0.01. In addition to the fact that the equivalence ratios at extinction for the airplane experiments with CH$_4$/air mixtures agreed within ± 5 % to the results from the droptower experiments for the same mixture by our previous study with the same setup [14], the experimental results are regarded to be reliable. However, for the Xe mixtures, there are large scatterings among the extinction points. For example, extinction was observed at $\phi = 0.35$ and 0.41 for $a = 1.9$ s^{-1} in two different experiments. In these conditions, the near-limit flames were planar flames with receding edges. Once these flames are formed, it is likely that the Lewis number effect and the large curvature of the flame before extinction acts to alter the deterministic nature of the steady deflagration wave. This leads to the large scattering of the extinction points for Xe mixtures. In addition, flame extinction was observed at $\phi = 0.43$ and $a = 1.1$ s^{-1}. However,

for a slightly lower stretch rate condition of $a = 0.80$ s^{-1}, extinction was observed at $\phi = 0.37$, which is very different from the one-dimensional computational results of around $\phi = 0.50$ at $a = 0.8$ s^{-1}. In these conditions, sporadic flames were observed experimentally which indicate that the formation of sporadic flames near the combustion limit caused the flame regime to extend far beyond the computational extinction boundary obtained by the one-dimensional computations
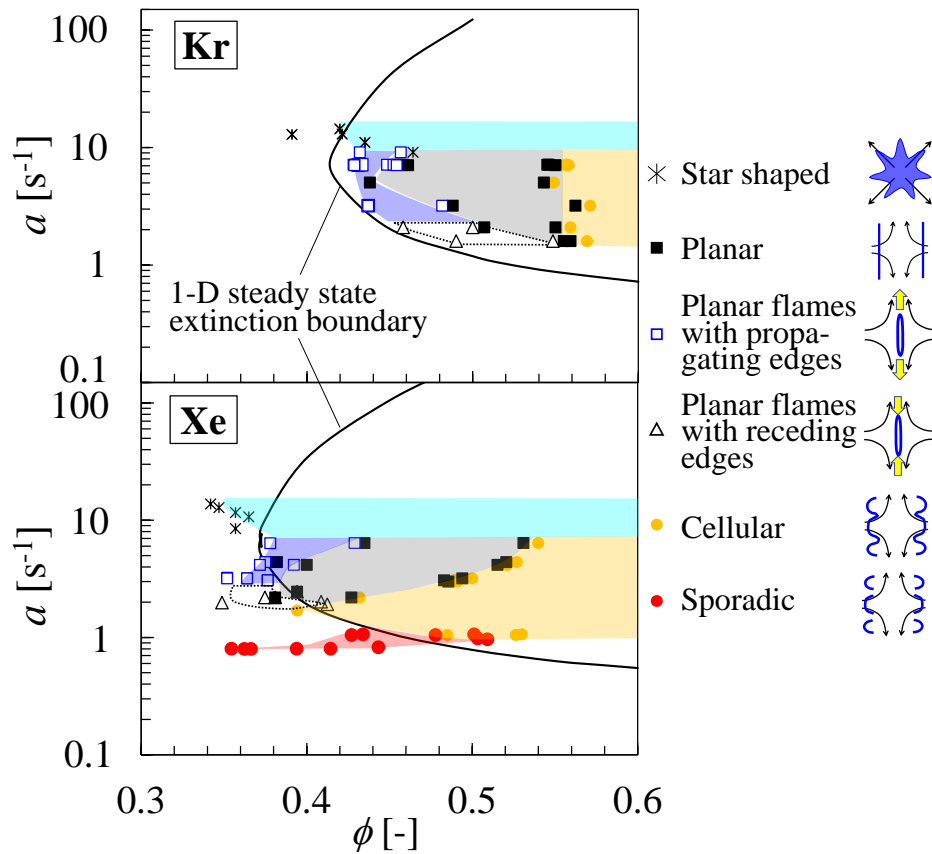

Fig. 10 Experimental flame regimes shown with the extinction boundaries (—) obtained by the one-dimensional computations with the PREMIX-based code using detailed chemistry for Kr and Xe mixtures. ✳ are star-shaped flames, ■ are planar flames, □ are planar flames with propagating edges, △ are planar flames with receding edges, ● are cellular flames, ● are sporadic flames.

with the PREMIX-based code using detailed chemistry. This is the indication of the broken C-shaped extinction curve.

Figure 11 shows the computational flame regime diagram obtained in the three-dimensional computations with the thermal-diffusion model using an overall one-step reaction for counterflow flames in the non-dimensional and dimensional parameter values. In the non-dimensional regime diagram, the horizontal axis is plotted as a function of $1/\sigma-1$ since $1/\sigma-1=T_b/T_0-1$ can uniquely characterize the fuel concentration in the unburnt gas mixture. The flame types at either steady states or quasi-steady states are plotted in the flame regime diagram. The extinction boundary obtained by the one-dimensional computations with the thermal-diffusion model using an overall one-step reaction and the combustion limit of the flame ball obtained with the three-dimensional computations using an overall one-step reaction are also shown in Fig. 11.

At $Le = 0.75$ which is roughly equivalent to Kr mixtures in the experiments, only planar

flames are formed and the computational extinction boundary obtained by the three-dimensional

computations agree with that obtained by the one-dimensional computations. Since the extinction

points obtained in the experiments and the three-dimensional computations agreed with the one-

dimensional computations, it is both experimentally and computationally shown that the one-
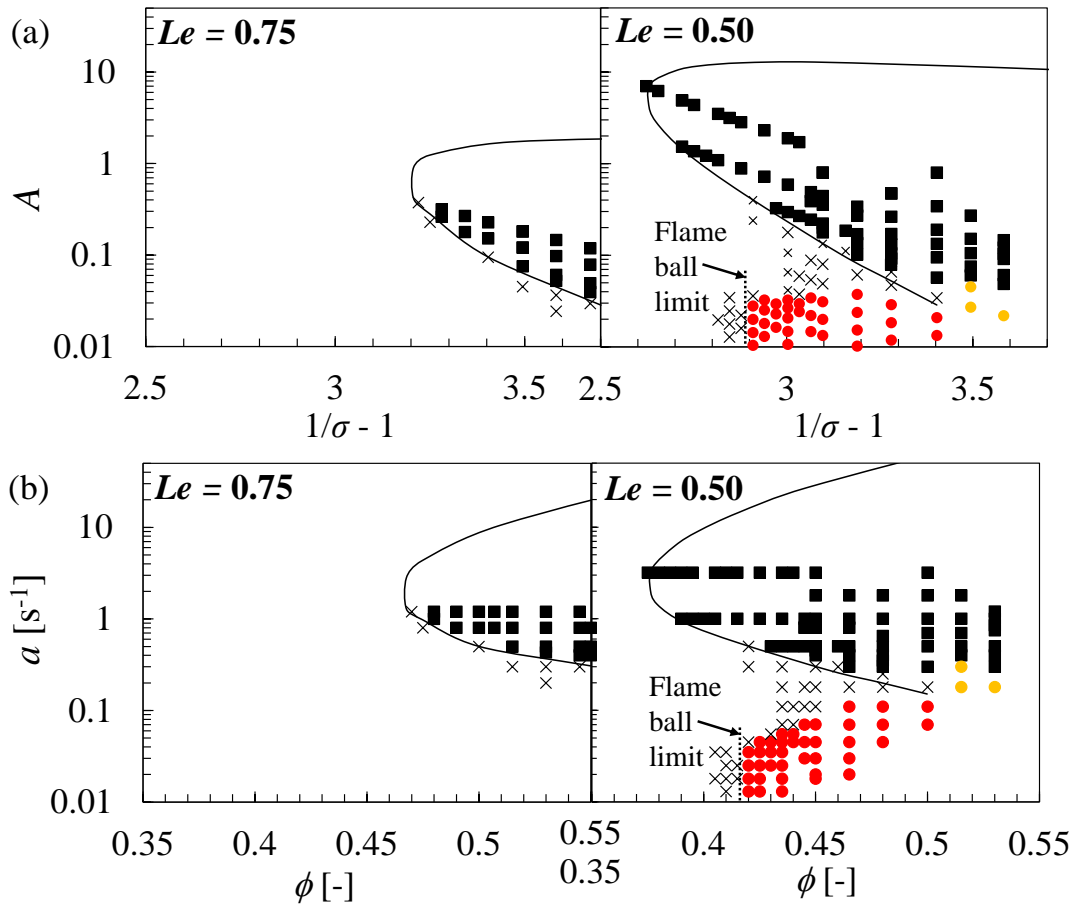

Fig. 11 Computational flame regimes and the extinction boundaries (—) obtained by the three-dimensional and one-dimensional computations with the thermal-diffusion model using an overall one-step reaction in non-dimensional parameters (a) and dimensional parameters (b). ■ indicate planar flames, 🟡 indicate cellular flames, 🔴 indicate sporadic flames, ✕ indicate extinction.

dimensional modeling is sufficient to obtain the accurate extinction points for conditions around

$Le = 0.75$. Note that different behavior of the edges of the planar flames seen in the experiments

were not observed in the computations. This is likely due to the coupled effect of the initial

condition, and the mixture being introduced along the entire computational boundary in the

present computations. Neither cellular flames nor star-shaped flames are observed in the three-

dimensional computations at $Le = 0.75$.

On the other hand, at $Le = 0.50$ which is roughly equivalent to Xe mixtures in the

experiments, planar flames, cellular flames, and sporadic flames are observed in the three-

dimensional computations with the thermal-diffusion model using an overall one-step reaction.

Cellular flames are observed at relatively high equivalence ratio and low stretch rate conditions,

which is in qualitative agreement with the experimental flame regime of cellular flames for Xe

mixtures. Sporadic flames are seen at the conditions outside of the extinction boundary of the

one-dimensional computations at $A < 0.037$ and $\phi > 0.415$. The figure with the non-dimensional

parameters showed the existence of a specific non-dimensional stretch rate limit in the region of

sporadic flames which are in good correspondence with the observation in [12] and the theoretical

prediction in divergent channels [26] that the flame propagation velocity of the sporadic flame

remains almost constant regardless of the stretch rate. The region of the sporadic flame and the

deviation of the C-shaped extinction boundary from the C-shaped extinction boundary in this

region qualitatively agrees to the experimental results. Interestingly, the lean combustion limit of the sporadic flame is very close to the lean combustion limit of the flame ball ($\sigma = 0.2583$ equivalent to $\phi = 0.414$) obtained with the three-dimensional thermal-diffusion model in the present computations. This indicates that the combustion limit of the sporadic flame may asymptote to the combustion limit of the flame ball. The upper Lewis number limit for flame balls were also around $Le = 0.65$ in the present computations. Since sporadic flames are the intermediate combustion modes between flame balls and propagating flames, the reason why the sporadic flames were not observed at $Le = 0.75$ is because the flame ball solution does not exist at $Le = 0.75$ for the current condition. For both $Le = 0.75$ and $Le = 0.50$ mixtures, quantitative agreement is not obtained between the experimental and the computational flame regimes. Possible causes include the interaction between the flame and the flow field, and the inaccuracy of the employed chemical model which may be a direction for investigations in the future.

7. Conclusions

In this study, experiments on counterflow flames for $CH_4/O_2/Kr$ ($Le \approx 0.7$–0.8) and $CH_4/O_2/Xe$ ($Le \approx 0.5$) mixtures under microgravity were conducted to examine the effect of Lewis number on the extinction boundary, flame regimes, and the formation of sporadic flames. Three types of computations were conducted, which are one-dimensional computations using detailed

chemistry with a PREMIX-based code, and three- and one-dimensional computations with the

thermal-diffusion model using an overall one-step reaction, to compare with the experimental and

computational results.

In the microgravity experiments at $\phi = 0.42$, planar flames, cellular flames, and sporadic

flames were observed with the decrease in stretch rate for Xe mixtures, while only planar flames

were observed for Kr mixtures. The flame types obtained in the three-dimensional computations

with the thermal-diffusion model using an overall one-step reaction for counterflow flames

showed qualitative agreement to the experimental results at the same equivalence ratio conditions

of $\phi = 0.42$. In the microgravity experiments, planar circular flames with receding edges, planar

circular flames with propagating edges, and star-shaped flames were observed.

Comparison between the sporadic flames obtained with the three-dimensional

computations and the flame balls obtained with the same thermal-diffusion model showed that

sporadic flames have slightly smaller characteristic flame sizes than the flame ball in the axial

direction, but have larger characteristic flame sizes in the direction parallel to the stagnation plane.

In addition, the stretch rate dependence of the characteristic flame size for sporadic flames, and

the similarity in fuel concentration dependence of the characteristic flame sizes for sporadic

flames and flame balls strongly indicated that sporadic flames are intermediate combustion modes

that segue flame balls to propagating flames.

The extinction boundary in the experimental flame regime diagram for Kr mixtures showed qualitative agreement to the computational regime diagram at $Le = 0.75$. Also, the regime of cellular and sporadic flames and the extinction boundary in the experimental flame regime diagram for Xe mixtures showed qualitative agreement to the computational regime diagram at $Le = 0.50$. The lean combustion limit of sporadic flames was shown to agree with that of the flame ball. This indicated that the disappearance of the regime of sporadic flames for $Le = 0.75$ mixtures is due to the Lewis number limit of the flame ball, which was obtained to be around $Le = 0.65$ in the current conditions with the thermal-diffusion model.

8. References

[1]   C.K. Law, S. Ishizuka, M. Mizomoto, Lean-limit extinction of propane/air mixtures in the stagnation-point flow, Symp. (Int.) Combust. 18 (1981) 1791–1798.

[2]   S. Ishizuka, C.K. Law, An experimental study on extinction and stability of stretched premixed flames, Symp. (Int.) Combust. 19 (1982) 327–335.

[3]   J. Sato, Effects of Lewis number on extinction behavior of premixed flames in a stagnation flow, Symp. (Int.) Combust. 19 (1982) 1541–1548.

[4]   S.H. Sohrab, C.K. Law, Extinction of premixed flames by stretch and radiative loss, Int. J. Heat Mass Transf. 27 (1984) 291–300.

[5]   S.H. Sohrab, Z.Y. Ye, C.K. Law, Theory of interactive combustion of counterflow

premixed flames, Combust. Sci. Technol. 45 (1986) 27–45.

[6]   C.J. Sung, C.K. Law, Extinction mechanisms of near-limit premixed flames and extended

limits of flammability, Symp. (Int.) Combust. 26 (1996) 865–873.

[7]   K. Maruta, M. Yoshida, Y. Ju, T. Nioka, Experimental study on methane-air premixed

flame extinction at small stretch rates in microgravity, Symp. (Int.) Combust. 26 (1996)

1283–1289.

[8]   J. Buckmaster, The effects of radiation on stretched flames, Combust. Theory Model. 1

(1997) 1–11.

[9]   H. Guo, Y. Ju, K. Maruta, T. Nioka, F. Liu, Radiation extinction limit of counterflow

premixed lean methane-air flames, Combust. Flame. 109 (1997) 639–646.

[10] Y. Ju, H. Guo, K. Maruta, F. Liu, On the extinction limit and flammability limit of non-

adiabatic stretched methane–air premixed flames, J. Fluid Mech. 342 (1997) 315–334.

[11] K. Takase, X. Li, H. Nakamura, T. Tezuka, S. Hasegawa, M. Katsuta, M. Kikuchi, K.

Maruta, Extinction characteristics of CH4/O2/Xe radiative counterflow planar premixed

flames and their transition to ball-like flames, Combust. Flame. 160 (2013) 1235–1241.

[12] R. Fursenko, S. Minaev, H. Nakamura, T. Tezuka, S. Hasegawa, K. Takase, X. Li, M.

Katsuta, M. Kikuchi, K. Maruta, Cellular and sporadic flame regimes of low-Lewis-

number stretched premixed flames, Proc. Combust. Inst. 34 (2013) 981–988.

[13]   R. Fursenko, S. Minaev, H. Nakamura, T. Tezuka, S. Hasegawa, T. Kobayashi, K. Takase,

M. Katsuta, M. Kikuchi, K. Maruta, Near-lean limit combustion regimes of low-Lewis-

number stretched premixed flames, Combust. Flame. 162 (2015) 1712–1718.

[14]   T. Okuno, H. Nakamura, T. Tezuka, S. Hasegawa, K. Takase, M. Katsuta, M. Kikuchi, K.

Maruta, Study on the combustion limit, near-limit extinction boundary, and flame regimes

of low-Lewis-number CH4/O2/CO2 counterflow flames under microgravity, Combust.

Flame. 172 (2016) 13–19.

[15]   L. Kagan, G. Sivashinsky, Self-fragmentation of nonadiabatic cellular flames, Combust.

Flame. 108 (1997) 220–226.

[16]   I. Brailovsky, G.I. Sivashinsky, On stationary and travelling flame balls, Combust. Flame.

110 (1997) 524–529.

[17]   L. Kagan, S. Minaev, G. Sivashinsky, On Disintegration of Cellular Flames, Lect. Notes

Comput. Sci. 2668 (2003) 811–818.

[18]   F.A. Williams, J.F. Grcar, A hypothetical burning-velocity formula for very lean

hydrogen-air mixtures, Proc. Combust. Inst. 32 I (2009) 1351–1357.

[19]   S. Minaev, L. Kagan, G. Joulin, G. Sivashinsky, On self-drifting flame balls, Combust.

Theory Model. 5 (2000) 609–622.

[20]   S.S. Minaev, L. Kagan, G. Sivashinsky, Self-propagation of a diffuse combustion spot in premixed gases, Combust. Explos. Shock Waves. 38 (2002) 9–18.

[21]   L. Kagan, S. Minaev, G. Sivashinsky, On self-drifting flame balls, Math. Comput. Simul. 65 (2004) 511–520.

[22]   Y.L. Shoshin, L.P.H. d. Goey, Experimental study of lean flammability limits of methane/hydrogen/air mixtures in tubes of different diameters, Exp. Therm. Fluid Sci. 34 (2010) 373–380.

[23]   Y.L. Shoshin, J.A. Van Oijen, A. V. Sepman, L.P.H. De Goey, Experimental and computational study of the transition to the flame ball regime at normal gravity, Proc. Combust. Inst. 33 (2011) 1211–1218.

[24]   F.E. Hernández-Pérez, B. Oostenrijk, Y. Shoshin, J.A. van Oijen, L.P.H. de Goey, Formation, prediction and analysis of stationary and stable ball-like flames at ultra-lean and normal-gravity conditions, Combust. Flame. 162 (2015) 932–943.

[25]   Z. Zhou, Y. Shoshin, F.E. Hernández-Pérez, J.A. van Oijen, L.P.H. de Goey, Effect of pressure on the lean limit flames of H2-CH4-air mixture in tubes, Combust. Flame. 183 (2017) 113–125.

[26]   R. Fursenko, S. Minaev, Flame balls dynamics in divergent channel, Combust. Theory Model. 15 (2011) 817–825.

[27] X. Chen, Z. Lu, S. Wang, Near limit premixed flamelets in Hele-Shaw cells, Proc. Combust. Inst. 36 (2017) 1585–1593.

[28] Y.B. Zel'dovich, G.I. Barenblatt, V.B. Librovich, G.M. Makhviladeze, The Mathematical Theory of Combustion and Explosions, Consultants Bureau, New York, 1985.

[29] J. Buckmaster, G. Joulin, P. Ronney, The structure and stability of nonadiabatic flame balls, Combust. Flame. 79 (1990) 381–392.

[30] J.D. Buckmaster, G. Joulin, P.D. Ronney, The structure and stability of nonadiabatic flame balls: II. Effects of far-field losses, Combust. Flame. 84 (1991) 411–422.

[31] C.J. Lee, J. Buckmaster, The Structure and Stability of Flame Balls: A Near-Equidiffusional Flame Analysis, SIAM J. Appl. Math. 51 (1991) 1315–1326.

[32] J. Buckmaster, M. Smooke, V. Giovangigli, Analytical and numerical modeling of flame-balls in hydrogen-air mixtures, Combust. Flame. 94 (1993) 113–124.

[33] M.S. Wu, J.B. Liu, P.D. Ronney, Numerical simulation of diluent effects on flame balls, Symp. (Int.) Combust. 27 (1998) 2543–2550.

[34] M. Abid, M.S. Wu, J.B. Liu, P.D. Ronney, M. Ueki, K. Maruta, H. Kobayashi, T. Niioka, D.M. Vanzandt, Experimental and numerical study of flame ball IR and UV emissions, Combust. Flame. 116 (1999) 348–359.

[35] M.S. Wu, P.D. Ronney, R.O. Colantonio, D.M. Vanzandt, Detailed numerical simulation

of flame ball structure and dynamics, Combust. Flame. 116 (1999) 387–397.

[36] P.D. Ronney, Near-limit flame structures at low Lewis number, Combust. Flame. 82 (1990) 1–14.

[37] P.D. Ronney, M.-S. Wu, H.G. Pearlman, K.J. Weiland, Experimental study of flame balls in space: Preliminary results from STS-83, AIAA J. 36 (1998) 1361–1368.

[38] Diamond Air Service Incorporation. http://www.das.co.jp/en/index.html (accessed October 6, 2017).

[39] G.P. Smith, D.M. Golden, M. Frenklach, N.W. Moriarty, B. Eiteneer, M. Goldenberg, C.T. Bowman, R.K. Hanson, S. Song, W.C. Gardiner Jr., V.V. Lissianski, Z. Qin, GRI-Mech 3.0, (2002). http://combustion.berkeley.edu/gri-mech/ (accessed October 6, 2017).

[40] NIST Chemistry WebBook, (2017). http://webbook.nist.gov/chemistry/ (accessed October 10, 2017).

[41] W.J. Moore, Physical Chemistry, Tokyo Kagaku Dojin, Japan, 1974.

[42] T. Okuno, H. Nakamura, T. Tezuka, S. Hasegawa, K. Maruta, Ultra-lean combustion characteristics of premixed methane flames in a micro flow reactor with a controlled temperature profile, Proc. Combust. Inst. 36 (2017) 4227–4233.

[43] J.S. Park, D.J. Hwang, J. Park, J.S. Kim, S. Kim, S.I. Keel, T.K. Kim, D.S. Noh, Edge flame instability in low-strain-rate counterflow diffusion flames, Combust. Flame. 146

(2006) 612–619.

[44]   D.G. Park, J.H. Yun, J. Park, S.I. Keel, A study on flame extinction characteristics along

a C-curve, Energy and Fuels. 23 (2009) 4236–4244.

[45]   Z. Lu, J. Buckmaster, Interactions of flame balls, Combust. Theory Model. 12 (2008) 699–

715.

[46]   A.W. Fitzgibbon, R.B. Fisher, F. Hill, E. Eh, Direct Least Squres Fitting of Ellipses, IEEE

Trans. Pattern Anal. Mach. Intell. 21 (1996) 1–15.

[47]   S. Beucher, C. Lantuéjoul, Use of Watersheds in Contour Detection, Rennes, France, 1979.

[48]   W. Gerlinger, K. Schneider, H. Bockhorn, Numerical simulation of three-dimensional

instabilities of spherical flame structures, Proc. Combust. Inst. 28 (2000) 793–799.

[49]   W. Gerlinger, K. Schneider, J. Fröhlich, H. Bockhorn, Numerical simulations on the

stability of spherical flame structures, Combust. Flame. 132 (2003) 247–271.